PROPERTIES OF THE COMPOSITES MADE OF GLAUCONITE AND POLYANILINE IN AQUEOUS SOLUTIONS OF PHOSPHORIC ACID

Solomiia Nesterivska[1], Victoriia Makogon[1], Mykhaylo Yatsyshyn[1, ✉], Ivan Saldan[1], Oleksandr Reshetnyak[1], Nestor German[1], Yurii Stadnyk[1]

Abstract. The glauconite-polyaniline composites were prepared through oxidation of aniline using ammonium peroxodisulfate in aqueous solutions of phosphoric acid on the surface of a glauconite powder. Intermolecular interaction between amorphous polyaniline macromolecules and interphase coupling of polyaniline to the glauconite surface was confirmed by X-ray diffraction and FT-IR spectroscopy. Higher concentration of phosphoric acid led to a stronger intermolecular and interphase connection because of H-bonding, and that resulted in higher electric conductivity while a magnetic susceptibility of the composites was not affected. Thermal analysis for the prepared composites confirmed the interfacial interaction between the polyaniline macromolecules and the surface of powdered glauconite.

Keywords: glauconite-polyaniline composite, structure, electric conductivity, magnetic susceptibility, thermal stability.

1. Introduction

Preparation and characterisation of composite materials made of organic polymer and inorganic substances have been an important scientific problem for quite a time [1, 2]. Among a huge variety of such materials, the composites where inorganic component is natural or clay mineral (NM or CM, respectively) attract special attention. In most cases, NM are aluminosilicates constructed from a different number of nanosized layers of $[AlO_3(OH)_3]^{6-}$ octahedrons (O) and layers of so-called $[SiO_4]^{4-}$ tetrahedra (T) packages, separated by emptiness filled by hydrated ions (mainly Na^+ and Ca^{2+}), for example, montmorillonite (T–O–T) or kaolin/kaolinite (T–O) [5].

The emptiness between the parallel aluminosilicate layers has become an important construction element that is particularly desirable for intercalated composites [5].

Among organic components for composites, nonelectroconductive polymers were studied more extensively as compared to the electroconductive ones [2-4]. Also, polyaniline (PAn) as one of the most popular electrocunductive organic polymers started to be used for composite preparation [5]. In addition to functional properties of the prepared composite [6], the usage of these cunductive polymers results in higher electric conductivity and even mechanical stability [7]. Depending on the NM nature and method of NM-PAn composite preparation, they are divided into three groups: 1) unmixed, or phase separated; 2) intercalated; and 3) delaminated composites [5]. Impregnation of NMs in aqueous solutions of acids, usually taken for the composite preparation, leads to the negative charge of their surface, providing for cation adsorption of aniline and promoting delimination of NMs [8]. Therefore, the ratio between PAn and NM should be accountable for the structure and properties of the prepared composites [5]. In addition to that, additive screening aimed at controlling PAn properties is also very much advisable [9].

Glauconite (G) is a very well studied NM, it belongs to the group of hydromicas of laminated silicates subclass and is considered to be aqueous aluminosilicate of potassium, magnesium and iron [10]. It is a globally popular mineral with quite a high content in rock (70–80 %). It was not used as inorganic component during composite preparation till 2010 [11], most probably, because of difficulties with cleaning it from impurities [12]. Recently, G-PAn composites preparation has been carried out using mechanochemical [13] or chemical methods [14-20] with different content of inorganic component and several aqueous solutions of acid-dopants for PAn (*e.g.* chloride [14], sulfate [15], phosphoric [16], oxalate [17], apple [18], and citric acids [19, 20]).

[1] Ivan Franko National University of Lviv,
6, Kyryla & Mefodiya St., 79005 Lviv, Ukraine
✉ *mykhaylo.yatsyshyn@lnu.edu.ua*

Ammonium peroxodisulfate was used as an oxidizer for aniline. Comparative analyses of the structural, thermal, electrical and magnetic properties of the composites were carried out in [11-22]. These studies suggest mainly amorphous PAn with 1,4-binding of aniline molecules in their macromolecular chains, and also availbiltiy of interphase connection between G and PAn. Higher values of electric conductivity for G-PAn composites were found in the case when acid-dopants were used [21]. Since phosphoric acid can be considered as a stable acid-dopant for PAn, it might be used during both electrochemical [23, 24] and chemical synthesis of PAn [25-30], as well as G-PAn composite preparation using a chemical method [31-33].

The present work is a continuation of G-PAn composite optimisation regarding their structure, electric conductivity, and magnetic susceptibility.

2. Experimental

2.1. Reagents and Materials

Aniline ($C_6H_5NH_2$, 99%), ammonium peroxo-disulfate (($NH_4)_2S_2O_8$, 98%), and phosphoric acid (H_3PO_4, 85%) were delivered from Sigma Aldrich. Distilled water was used as a solvent during all chemical syntheses. G (97-98%, average particle size ≤20 μ) was taken for the composite preparation as in [22]. The mass ratio between G and PAn was 1:1.

2.2. G-PAn Composite Preparation

PAn and G-PAn samples were obtained through chemical oxidation of aniline by ammonium peroxodisulfate in aqueous solutions of phosphoric acid (0.1, 0.5, 1.0 or 2.0 M, Table 1). Molar ration between aniline and ammonium peroxodisulfate was 1:1.1. G (1 g) was added to 80 ml of aniline in phosphoric acid and stirred at 293 K for 1 h and then untrasonicated for 10 min. Ammonium peroxodisulfate (20 ml) in phosphoric acid was dripped into aniline solution or G suspension in aniline during stirring for 1 h, followed by continuous stirring of the prepared mixtures for another 1 h. The obtained composites were kept for a day, and then filtered and washed with distilled water till the neutral pH value. Finally, they were dried in vacum (1–10 Pa) at 333 K during 24 h and crushed in a porcelain mortar.

2.3. Materials Characterisation

Powder X-ray diffraction (XRD) patterns were collected using Cu Kα radiation (1.54056 Å) at the voltage of 40 kV and beam current of 40 mA on a DRON-4-07 instrument. The samples were deposited on a zero background Si sample holder. Data acquisition was performed with a step size of 0.02º and 7 s/step measurement time within the 2θ range of 5–50º.

Fourier transform infrared (FT-IR) spectroscopy was used for detecting organic functional groups within the wavenumber range of 4000–650 cm^{-1}. The FT-IR measurements were performed in a transmittance mode with a NICOLET iS10 instrument, THERMO SCIENTIFIC. Data exposition was taken in 256 scans at the resolution of 4 cm^{-1} and data spacing of 0.482 cm^{-1}. For each sample, a collected background (FT-IR for an empty sample holder) was measured to make spectral subtraction in the same conditions.

Values of electric conductivity were calculated according to the method described in detail in [34]. Magnetic susceptibility was obtained through Faraday approach using EM-5-ZMP microbalance [35] within the magnetic field from 100 to 900 kA·m^{-1} and vacuum of 0.1 Pa at 293±1 K [20].

Thermal analysis of powdered samples was performed using a Q1500-D derivatograph (IOM, Hungary) in the temperature range of 293–1173 K with a heating rate of 10 K/min in air. Standard Al_2O_3 crucibles filled with a sample weight of 100 mg were used. Thermogravimetry (TG) including differential thermal analysis (DTA) and differential thermogravimetry (DTG) was applied to estimate the effect of temperature and chemical composition on thermal stability of the prepared G-PAn composites.

Table 1

**PAn and G-PAn samples prepared
in aqueous solution of phosphoric acid**

Symbols for samples	$C(H_3PO_4)$, M	Sample output, ±0.5 %
PAn (0.1)	0.1	86.6
G-PAn (0.1)		71.4
PAn (0.5)	0.5	93.5
G-PAn (0.5)		78.5
PAn (1.0)	1.0	99.1
G-PAn (1.0)		84.8
PAn (2.0)	2.0	99.5
G-PAn (2.0)		89.1

3. Results and Discussion

3.1. The Structure of the Prepared PAn and G-PAn Composites

Prepared PAn and G-PAn samples contained PAn doped by phosphoric acid. Sample output is within the range of ~71–99 % and correlates well with an acid concentration value, though the output of G-PAn is lower as compared to those of PAn samples (Table 1). Increase in phosphoric acid content results in higher values of the output for both PAn and G-PAn samples. XRD for PAn (0.1) sample suggests an amorphous material (Fig. 1a, *curve 1*), while for PAn (0.5), PAn (1.0) and PAn (2.0) (Fig.1a, *curves 2-4*) two sharp peaks at $2\theta = 20.70°$ and $2\theta = 25.29°$ can be traced, in addition to a wide amorphous halo. Most probably, they mean periodic crystalline regions that correspond to parallel and perpendicular orientations of macromolecular PAn chains [14, 15, 20, 22, 23, 31] inside their amorphous array. For all samples, PAn is considered in two forms – emeraldine base (EB) and salt (ES) of phosphoric acid [14, 15, 20, 22, 29, 31, 36]. XRD pattern for PAn (0.1) is a bit different from others (Fig 1a) since the peak position responsible for EB in this sample is shifted to lower 2θ values and equals to 19.86°, as compared to 20.70° for other PAn samples. Higher intensity of the peak at 25.29° correlates with the increase in the $C(H_3PO_4)$ value, meaning higher crystallinity of PAn because of the increase in ES content.

Diffraction patterns for the prepared G-PAn composites (Fig.1b, *curves 1-4*) are quite similar to that of pure G (Fig.1b, *curve 5*) [14, 15, 22]. The most intense peaks at 2θ of 21.3° and 27.8° confirm the presence of G in the composites. Appearance of a weak diffraction peak at $2\theta = 5.88°$, which corresponds to T–O–T basal interplanar distance, might be considered as resulting from the existence of a partially intercatated composite. Additional small peak is visible at the position of 8.57, 8.97, 8.91 and 8.51°, for G-PAn (0.1), G-PAn (0.5), G-PAn (1.0) and G-PAn (2.0) composites, respectively.

A set of characteristic bands within the range of 4000–650 cm^{-1} for FT-IR spectra of PAn samples corresponds only to PAn [14-20, 22, 23, 26-30] (Fig. 2a). Low intensity bands at ~3220, ~3050 and ~2907 cm^{-1} might be attributed to H-bonding between macromolecular PAn chains with the involvement of amino (–NH–) and protonated amino (=N$^+$–) groups [28]. Broad and intense band within the range of 3400–1640 cm^{-1},

promoted by the appearance of (=N$^+$–) groups [28, 30], leads to the masking of the valence vibrations of –NH– and C–H groups of aromatic cycles as well as reflections of the H-bonding. The bands at 1567 and 1485 cm^{-1} (Fig. 2a, *curve 1*) correspond to valence vibrations of quinidine (*Q*) and benzenoid (*B*) component in PAn macromolecules, which is an important feature of PAn characterization/identification [14-20, 22, 23, 26-33]. Intense band at 1286 cm^{-1} is due to the vibrations of C–N bonds in *B* component, while a band at 1229 cm^{-1} and a shoulder at 1125 cm^{-1} correspond to valence vibrations of polar C–N$^{+\bullet}$ and C–N$^+$ bonds in *Q* component, respectively [14-20, 22, 23, 26-30, 33, 36, 38]. An increase in the $C(H_3PO_4)$ value results in a small shift (3–14 cm^{-1}) of the main characteristic bands towards lower wavenumbers (Table 2). This fact might be accounted for by amplification of the conjugation effect in macromolecular PAn chains because of acid-dopants [27, 31]. It should be noted that the increase in phosphoric acid concentration correlates with the ratio between intensities for a couple of peaks at ~1286 and ~1229 cm^{-1}. For example, for PAn (2.0) sample the intensities of these peaks are almost equal (Fig. 2a), confirming a higher protonation of C–N$^+$ groups in PAn macromolecules [36]. The observed broad band within the range of ~1200–900 cm^{-1} with the maximum at 1098 cm^{-1} is very similar to the value found in [27, 28, 33] and constitutes an integrity of several bands, in particular ~1125, ~1028 and ~965 cm^{-1}. These peak positions are referred to valence vibrations of C–N$^+$ bonds, as well as symmetric valence vibrations of sulfates (HSO$_4^-$ and SO$_4^{2-}$) as recovery products of ammonium peroxodisulfate reduction [27, 28, 36] and symmetric valence vibrations of phosphates (H$_2$PO$_4^-$ and HPO$_4^{2-}$) [27, 37] because of acid-dopants, respectively. The broadening of this band is caused by the protonation effect of (=N$^+$–) groups that are very sensitive to acid-dopant anions [27, 28, 33]. The intensity of sharp peak at ~1028 cm^{-1} decreases with the increase of $C(H_3PO_4)$ value and for PAn (2.0) sample becomes equal to that of the shoulder at 965 cm^{-1} (Fig. 2a, *curve 4*). Most probably, this fact is caused by H$_2$PO$_4^-$ groups in PAn. Since H$_2$SO$_4$ content in the sample did not change, the increase in $C(H_3PO_4)$ reduces pH value in the reaction mixtures. Therefore, the higher intensity of the shoulder at 1229 and 965 cm^{-1} occurs with the increase in $C(H_3PO_4)$ value. A small peak at ~795 cm^{-1} corresponds to out-of-plane deformation vibrations of C–H bonds of 1,4-substituted benzenoid cycles in macromolecular PAn chains [33, 36].

a)

b)

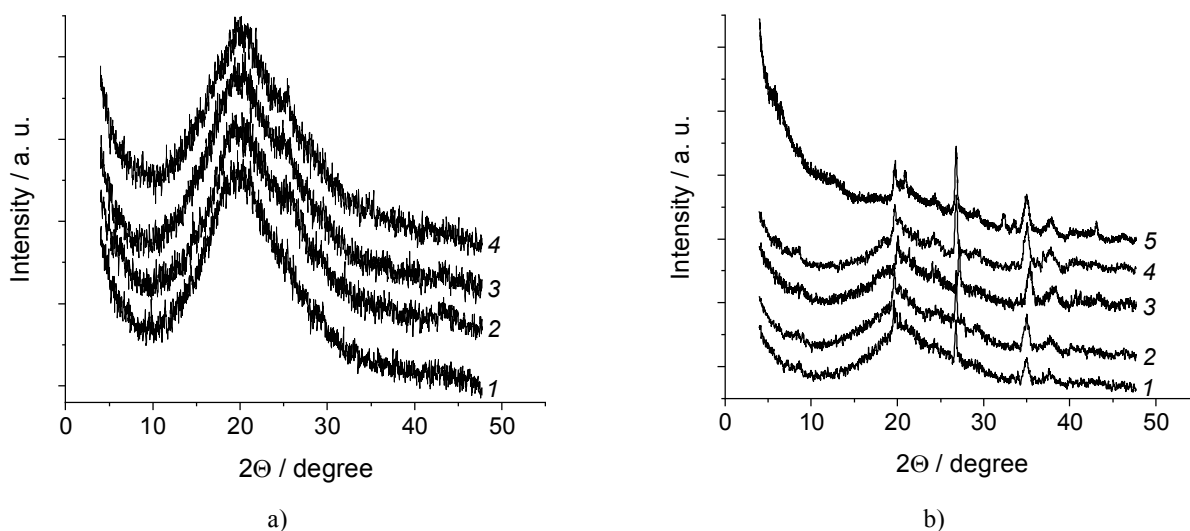**Fig. 1.** XRD for PAn (a) and glaucopnite-PAn composites (b). For (a): *1* – PAn (0.1); *2* – PAn (0.5); *3* – PAn (1.0); *4* – PAn (2.0). For (b): *1* – G-PAn (0.1); *2* – G-PAn (0.5); *3* – G-PAn (1.0); *4* – G-PAn (2.0); *5* – pure G
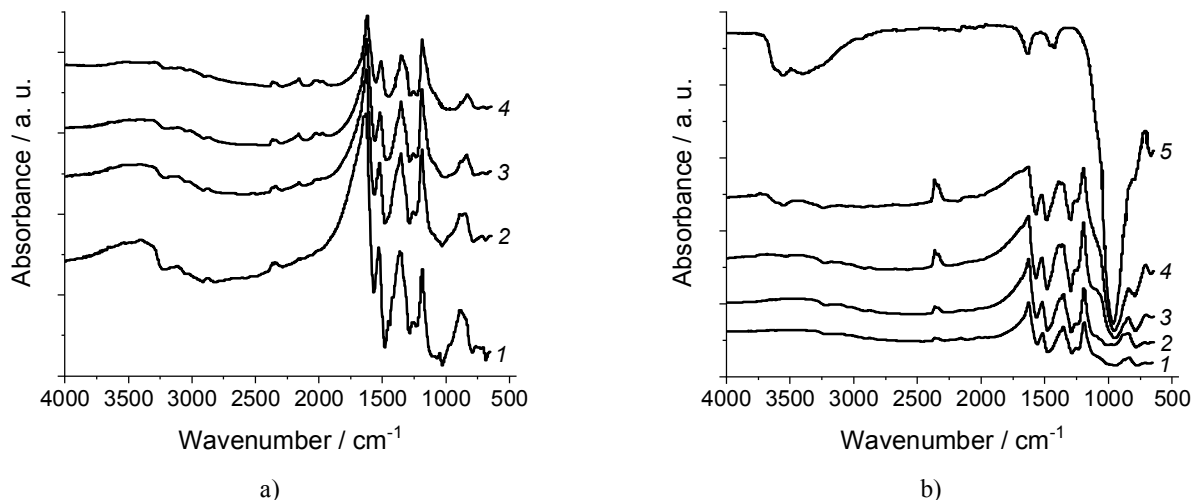

a)

b)

Fig. 2. FTIR spectra for PAn (a) and glaucopnite-PAn composites (b). For (a): *1* – PAn (0.1); *2* – PAn (0.5); *3* – PAn (1.0); *4* – PAn (2.0). For (b): *1* – G-PAn (0.1); *2* – G-PAn (0.5); *3* – G-PAn (1.0); *4* – G-PAn (2.0); *5* – pure G

Table 2

FT-IR spectra analysis of the prepared PAn and G-PAn composites

Sample	Wavenumber ± 1, cm^{-1}					
	N=Q=N^v	N−B−N^v	C−N^v	C−N$^{+\bullet\ v}$	C−N$^{+\ v}$	C−H^{op}
PAn (0.1)	1567	1485	1286	1233	1122	795
PAn (0.5)	1563	1480	1289	1239	1125	789
PAn (1.0)	1557	1444	1285	1235	1125	780
PAn (2.0)	1553	1444	1283	1232	1122	770
G-PAn (0.1)	1567	1485	1297	1234	1129	793
G-PAn (0.5)	1564	1481	1292	1242	1126	788
G-PAn (1.0)	1557	1479	1290	1240	1125	784
G-PAn (2.0)	1561	1481	1288	1239	1134	792

Notes: *s* is symmetric; *v* is valence; *p* is plane; *op* is out-of-plane; *Q* is quinidine and *B* is benzenoid cycle

FT-IR spectra for the prepared G-PAn composites are characterized by reflections of both PAn and G (Fig. 2b). The presence of G indicates the intensive characteristic band of pure G at 960 cm^{-1}, a bit shifted to ~950 cm^{-1} for the G-PAn composites. This peak is caused by valence vibrations of Si–O–Si and Al–O–Si groups as the main structural units of alumosilicates [16-20, 23, 39]. Absorption band at ~3630 cm^{-1} corresponds to Al–OH bonds, while that at ~3388 cm^{-1} – to Si–OH valence vibration [38, 39]. Two broad bands at 3588 and 3490 cm^{-1} correspond to surface –O–H groups which take part in the formation of H-bonding between PAn macromolecules [36]. The band at 3224 cm^{-1}, observed for both PAn and G-PAn samples (Fig. 2), might account for H-bonding in PAn and surface –O–H groups in G [36]. Small bands at 1638 and 1436 cm^{-1} in pure G account for surface adsorbed water [36, 39] and, probably, water linked between structural layers [40]. Therefore, these phenomena are not visible in case of G-PAn composites. The increase in intensity for the peak at ~960 cm^{-1}, especially for the samples with higher $C(H_3PO_4)$ value, might be accounted for by the overlapping of band for PAn, phosphates and sulphates with the intense band of G (Fig. 2b). This fact may also indicate the increased interaction between G and PAn [39, 41]. Higher ratio between intensity of the couple of peaks at ~1286 and ~1229 cm^{-1} in the composites might be caused by poor protonation of C–N$^+$ groups in PAn because of stronger H-bonding with the surface –O–H groups of G. The shoulders at ~1063 and ~800 cm^{-1} in FT-IR spectra of pure G might be attributed to the valence and deformative Si–O vibrations [33, 39]. Availability of characteristic bands for both G and PAn suggests formation of PAn on the surface of G powder during aniline polymerization.

3.2. Electric Conductivity of the Prepared PAn and G-PAn Composites

Since PAn is a well-known electroconductive organic polymer, prepared materials based on PAn might also be interesting due to their electric conductivity (σ) [5, 7, 9]. Calculated σ values for PAn and G-PAn samples are summarised in Table 3. Since G-PAn composites contain nonconductive G, their electric conductivity ((0.11–$0.61)\cdot10^{-2}$ S·cm^{-1}) is lower as compared to the corresponding PAn samples ((0.32–$3.93)\cdot10^{-2}$ S·cm^{-1}). For both PAn and G-PAn samples, the σ value becomes higher with the increase in $C(H_3PO_4)$ value [28, 31]. The obtained values of electric conductivity are similar to those of other composites [5, 7, 9].

Table 3

Electric conductivity of the prepared PAn and G-PAn composites

Sample	$\sigma \cdot 10^2 \pm 0.0005$, S·cm^{-1}
PAn (0.1)	0.32
PAn (0.5)	0.72
PAn (1.0)	1.59
PAn (2.0)	3.93
G-PAn (0.1)	0.11
G-PAn (0.5)	0.21
G-PAn (1.0)	0.39
G-PAn (2.0)	0.61

3.3. Magnetic Susceptibility of the Prepared PAn and G-PAn Composites

Since pure G is capable of being magnetized [35, 42], higher strength of magnetic field leads to higher value of magnetic susceptibility (Fig. 3, *curve 3*) [18, 20, 22]. Similar behavior has been confirmed experimentally for the prepared G-PAn (0.5) sample (Fig. 3, *curve 2*), while pure PAn is characterized by a very poor magnetic susceptibility that is almost independent of the magnetic field strength (Fig. 3, *curve 1*). It was found that $C(H_3PO_4)$ value does not influence the value of magnetic susceptibility of the prepared G-PAn composites.

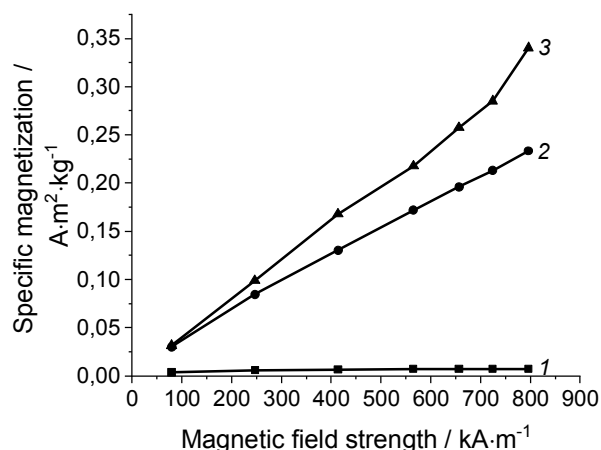**Fig. 3.** Magnetic susceptibility *vs*. magnetic field strength for pure PAn (*1*), G-PAn (0.5) composite (*2*) and pure G (*3*)

3.4. Thermal Stability of the Prepared PAn and G-PAn Composites

As usual thermal analysis of the prepared PAn and G-PAn composites is simplified to a few main stages using TG where DTG-, DSC- and DTA-curves are less commonly used. Sometimes masspectroscopy might be applied to analyse products of thermal destruction during thermal treatment [43, 44] that allows to suggest a decom-

position mechanism. Our measurements were focused on determination of the effect of phosphoric acid and G concentration on thermal properties of the prepared PAn and G-PAn composites using the approach described in [45].

TG- and DTG curves for pure PAn and G-PAn composites, as well as pure G, are shown in Fig. 4. Values of mass loss for every stage are collected in Tables 4 and 5. Detailed analysis of TG and DTG for PAn samples suggests three main stages of mass loss as minimum (Figs. 4a and 4c). TG curves for all PAn samples clearly show the minimum within temperature range of 303–463 K with the peak at ~353 K that corresponds to the loss of physically adsorbed water [43, 45]. The first minimum on DTG curves for G-PAn composites is shifted to 357.2 K that might be caused by G presence. The second minimum – in the temperature range of 463–693 K with peaks at 606.3, 604.7, 601.3 and 597.4 K for the composites doped with $C(H_3PO_4)$ of 0.1, 0.5, 1.0 and 2.0 M (Fig. 4d), respectively – is related to mass loss

because of phosphoric acid water solution and beginning of thermal destruction for PAn oligomeric molecules [43, 45, 46]. The third stage is traced in the range of 793–1123 K and is characterized by a broad peak centered with minimum at ~933 K that might be due to thermal and oxidative PAn destruction, as well decomposition of its products [45, 47]. The second minimum on DTG curves for PAn samples (Fig. 4c) transfers into the third one without going to the baseline that suggests overlopping on both stages [45, 47, 48]. For both PAn and G-PAn in the temperature range of 303–463 K the mass loss increases with the increase in $C(H_3PO_4)$ value that itself resulted in the higher amount of water stucked with acid-dopant (see Figs. 4a, 4b and Tables 4-5). Similar dependences were also found for second and third stages. Increase of $C(H_3PO_4)$ value from 0.1 to 2.0 M results in shift of complete water desorption from 447.42 to 471.10 K and from 448.34 to 460.00 K, respectively for the prepared PAn and G-PAn composites (Figs. 4c and 4d).
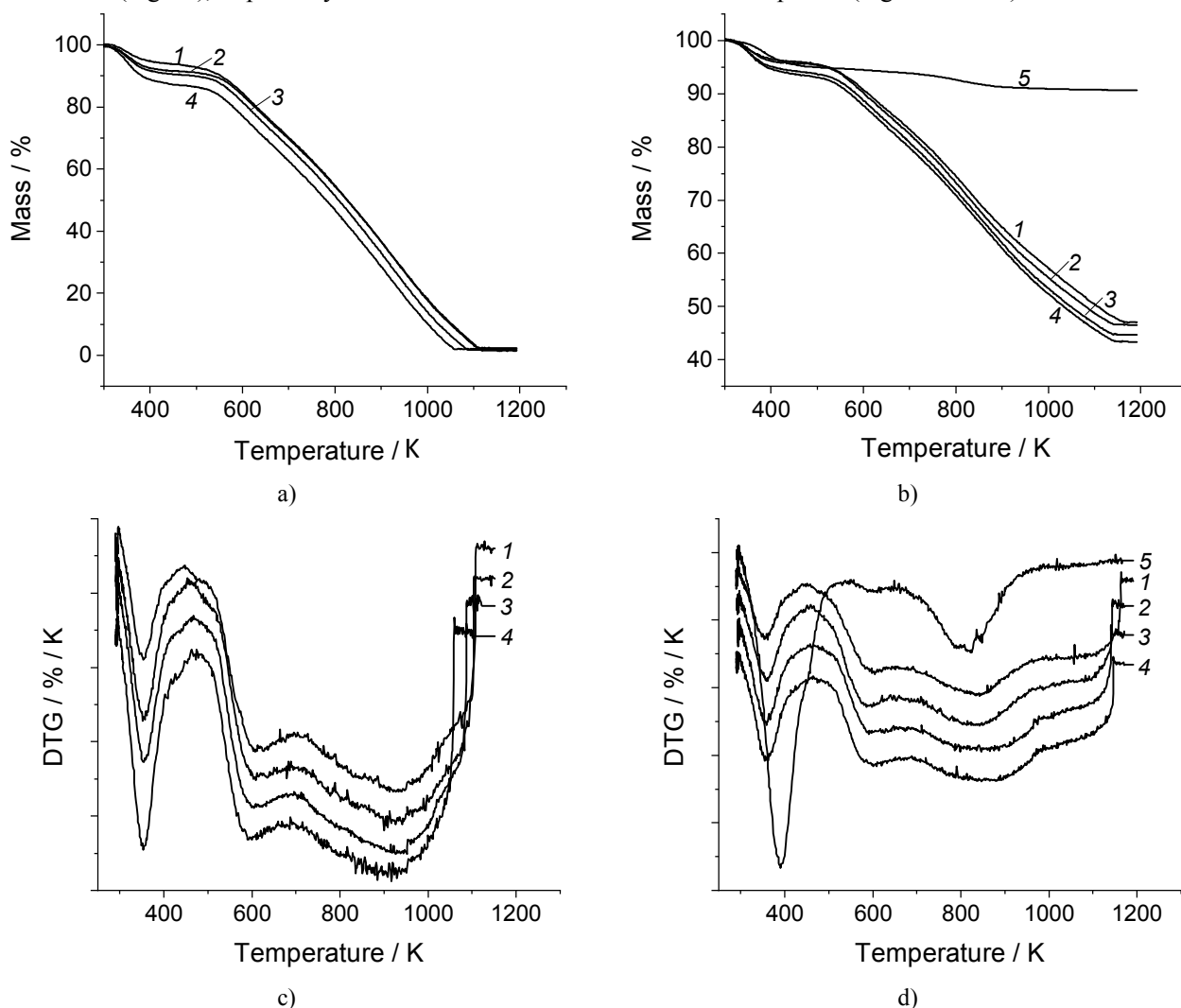

a)

b)

c)

d)

Fig. 4. TG- (a, b) and DTG- (c, d) curves for pure PAn (a, c) and G-PAn composites (b, d) doped with $C(H_3PO_4)$ of 0.1 M (1), 0.5 M (2), 1.0 M (3) and 2.0 M (4). The curves for pure G signed as (5) were used for the comparison

**Mass loss and final residue of the prepared PAn samples during their continuous thermal treatment
in air within the temperature range of 303-1123 K**

Sample	Mass loss, %				Final residue, %
	303–463 K	463–793 K	793–1123 K	303–1123 K	
PAn (0.1)	6.30	34.76	56.55	97.61	2.39
PAn (0.5)	8.53	35.88	54.06	98.47	1.53
PAn (1.0)	9.50	37.89	50.84	98.23	1.77
PAn (2.0)	12.96	39.11	45.89	97.96	2.04

**Mass loss and final residue of the prepared G-PAn composites during their continuous thermal treatment
in air within the temperature range of 303-1173 K**

Sample	Mass loss, %					Final residue, %
	303–460 K	460–665 K	665–985 K	985–1173 K	303–1173 K	
G-PAn (0.1)	3.95	18.71	11.29	19.09	53.04	46.96
G-PAn (0.5)	4.25	20.22	11.84	17.03	53.34	46.66
G-PAn (1.0)	5.78	20.27	14.27	14.98	55.30	44.70
G-PAn (2.0)	6.43	20.55	14.16	15.37	56.51	43.49

Two peaks at minimun of 390.22 and 600.73 K were found in DTG curves for pure G sample (in Fig. 4d, *curve 5*) that are due to water desorption from the surface and interlayer spaces, respectively. Broad peak within 653–983 K and centered at ~803 K conditioned by dehydroxilation of –OH groups from the surface of G in case of G-PAn composites with the formation of water [43]. For all G-PAn composites temperature values of release of adsorbed water and water solution of phosphoric acid (respectively, ~358 and ~603 K) and those that are responsible for water release from G are shifted to higher temperatures with the increase in $C(H_3PO_4)$ value. This behavior might suggest an interphase interaction between PAn macromolecules and surface of G powder. It should be mentioned that the total mass loss for PAn is around ~98 % (Fig. 4a) while for G-PAn composites it is approximately ~53–57 % and for pure G – only 9.37 % (Fig. 4b).

The shape of DTA curves (Fig. 5) confirms that the thermal destruction of the prepared PAn and G-PAn composites is an exothermic process [47, 49, 50] and suggests the change of specific heat capacity during heating [50]. For pure G dependence of specific heat capacity on temperature is not so pronounced (in Fig. 5b, *curve 5*). Small endothermic peaks at ~353 and ~504 K are found on DTA curves too. Exothermic maximum at temperature higher than 513 K corresponds to the onset of the thermal and oxidative destruction of PAn oligomeric molecules [45-50]. Broad endothermic peak within 773–1053 K corresponds to release of PAn decomposition products.
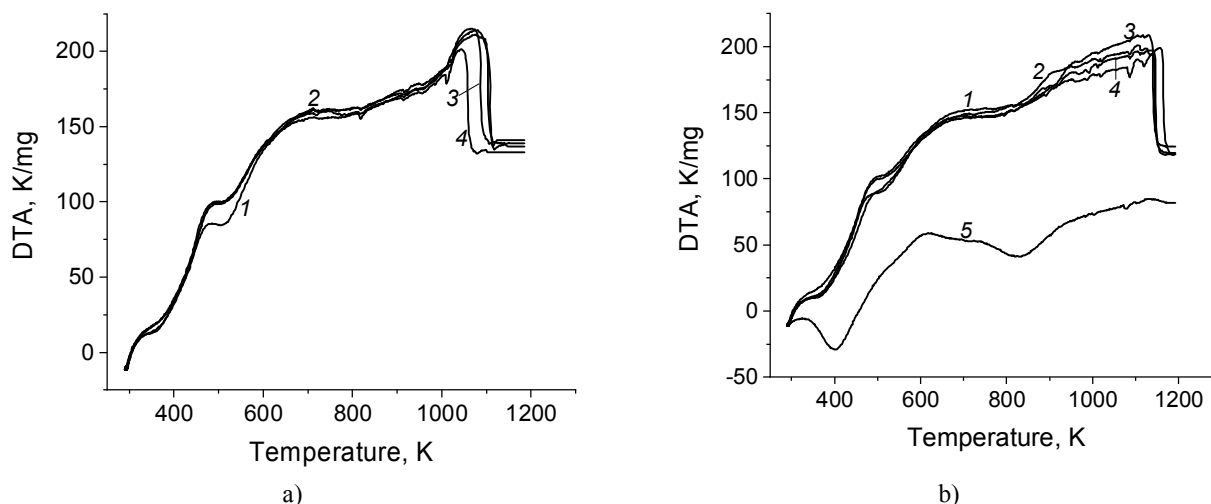

a)   b)

Fig. 5. TG curves for PAn (a) and G-PAn composites (b) doped with $C(H_3PO_4)$ of 0.1 M (1), 0.5 M (2), 1.0 M (3) and 2.0 M (4).
The curves for pure G signed as (5) were used for the comparison

Thermal analysis including TG-, DTG- and DTA-curves for the prepared PAn and G-PAn composites confirms that water desorption does not influence on PAn thermal and oxidative destruction [47]. For G-PAn composites the destruction happens in different temperature regions comparing to pure PAn. This suggests an effect of G powder on PAn macromolecule immobilisation [51] or formation of its branched structures [52].

4. Conclusions

PAn samples were prepared through oxidation reaction for aniline using ammonium peroxodisulfate in aqueous solutions of phosphoric acid. The same procedure with the addition of pure G was used for G-PAn composites preparation. XRD analysis suggests amorphous PAn samples, while additional crystalline peaks of G for the prepared composites can be traced. Because of H-bonding, intermolecular interaction between PAn macromolecules and interphase coupling of PAn to the surface of G powder were confirmed by FT-IR. It was found that higher concentration of phosphoric acid resulted in a stronger intermolecular and interphase connection. Electric conductivity of G-PAn composites was 3-6 times lower comparing to the corresponding PAn samples. Magnetic susceptibility of a G-PAn (0.5) composite showed a similar dependence on the magnetic field strength as for pure G. Increase in phosphoric acid concentration resulted in higher electric conductivity of all prepared samples, which does not affect their magnetic susceptibility. Thermal analysis including TG-, DTG- and DTA-curves for the prepared PAn and G-PAn composites suggest the interphase interaction between PAn macromolecules and the surface of G powder.

The prepared G-PAn composites might be recommended as effective adsorbers for high-density metals from aqueous solutions.

References

[1] Gomez-Romero P.: Adv. Mater., 2001, **13**, 163. https://doi.org/10.1002/1521-4095(200102)13:3<163::AID-ADMA163>3.0.CO;2-U
[2] Hussain F., Hojjati M., Okamoto M., Gorga R.: J. Composit. Mater., 2006, **40**, 1511. https://doi.org/10.1177/0021998306067321
[3] Utracki L., Sepehr M., Boccaleri E.: Polym. Adv. Technol., 2007, **18**, 1. https://doi.org/10.1002/pat.852
[4] Mittal V.: Materials, 2009, **2**, 992. https://doi.org/10.3390/ma2030992
[5] Makogon V., Yatsyshyn M., Reshetnyak O.: Pratsi Naukovoho Tovarystva im. Shevchenka. Khimichni nauky, 2017, **48**, 17.
[6] Malinauskas A.: Polymer, 2001, **42**, 3957. https://doi.org/10.1016/S0032-3861(00)00800-4

[7] Soundararajah Q., Karunaratne B., Rajapakse R.: Mater. Chem. Phys., 2009, **113**, 850. https://doi.org/10.1016/j.matchemphys.2008.08.055
[8] Liu D., Du X., Meng Y.: Mater. Lett., 2006, **60**, 1847. https://doi.org/10.1016/j.matlet.2005.12.033
[9] Ćirić-Marjanović G.: Synth. Met., 2013, **177**, 1. https://doi.org/10.1016/j.synthmet.2013.06.004
[10] Matkovs'kyi O., Pavlyshyn V., Slyvko Ye.: Osnovy Mineralohiyi Ukrayiny. Vydav. tsentr LNU im. Ivana Franka, Lviv 2009.
[11] Yatsyshyn M., Grynda Yu., Reshetnyak O. et al.: XVIth Int. Seminar on Physics and Chemistry of Solids. Lviv, June 2010, 151.
[12] Yatsyshyn M., Il'kiv Z., Halamay R. et al.: Pat. Ukraine 86632, Publ. Jan. 10, 2014.
[13] Yatsyshyn M., Stasiv N., Makogon V. et al.: Visnyk Lviv Univ. Ser. Chem. 2015, **56**, 388.
[14] Makogon V., Yatsyshyn M., Demchenko P.: Visnyk Lviv Univ. Ser. Chem., 2016, **57**, 471.
[15] Yatsyshyn M., Makogon V., Demchenko P. et al.: Visnyk Lviv Univ. Ser. Chem., 2015, **56**, 360.
[16] Makogon V., Nesterivs'ka S., German N., Yatsyshyn M.: Visnyk Lviv Univ. Ser. Chem., 2019, **60**, 360.
[17] Makogon V., Semenyuk Yu., Yatsyshyn M. et al.: Pratsi Naukovoho Tovarystva im. Shevchenka. Khimichni nauky, 2016, **44**, 57.
[18] Makogon V., Maksymiv N., Yatsyshyn M. et al.: Visnyk Lviv Univ. Ser. Chem., 2017, **58**, 412.
[19] Yatsyshyn M., Lytvyn Yu., Makogon V. et al.: Pratsi Naukovoho Tovarystva im. Shevchenka. Khimichni nauky, 2015, **42**, 72.
[20] Yatsyshyn M., Makogon V., Reshetnyak O. et al.: Chem. Chem. Technol., 2016, **10**, 429. https://doi.org/10.23939/chcht10.04.429
[21] Yatsyshyn M., Makogon V., Tsiko U., Reshetnyak O.: Pratsi Naukovoho Tovarystva im. Shevchenka. Khimichni nauky, 2019, **53**, 92.
[22] Yatsyshyn M., Saldan I., Milanese C. et al.: J. Polym. Environm., 2016, **24**, 196. https://doi.org/10.1007/s10924-016-0763-x
[23] Eftekhari A., Afshani R.: J. Polym. Sci. A, 2006, **44**, 3304. https://doi.org/10.1002/pola.21422
[24] Parsa A., Ab Ghani S.: Electrochim. Acta, 2009, **54**, 2856. https://doi.org/10.1016/j.electacta.2008.11.022
[25] Boara G., Sparpaglione M.: Synth. Met., 1995, **72**, 135. https://doi.org/10.1016/0379-6779(94)02337-X
[26] Kulkarni M., Viswanath A., Marimuthu R., Seth T.: Polym. Eng. Sci., 2004, **44**, 1676. https://doi.org/10.1002/pen.20167
[27] Blinova N., Stejskal J., Trchová M., Prokeš J.: Polymer, 2006, **47**, 42. https://doi.org/10.1016/j.polymer.2005.10.145
[28] Šeděnková I., Trchová M., Blinova N., Stejskal J.: Thin Solid Films, 2006, **515**, 1640. https://doi.org/10.1016/j.tsf.2006.05.038
[29] Sonawane Y., Kulkarni M., Kale B., Aiyer R.: Polym. Adv. Technol., 2008, **19**, 60. https://doi.org/10.1002/pat.974
[30] Wu J., Tang Q., Li Q., Lin J.: Polymer, 2008, **49**, 5262. https://doi.org/10.1016/j.polymer.2008.09.044
[31] Marins J., Soares B.: Synth. Met., 2012, **162**, 2087. https://doi.org/10.1016/j.synthmet.2012.10.015
[32] Marins J., Giulieri F., Soares B., Bossis G.: Synth. Met., 2013, **185-186**, 9. https://doi.org/10.1016/j.synthmet.2013.09.037
[33] Gu H., Guo J., Zhang X. et al.: J. Phys. Chem., 2013, **117**, 6426. https://doi.org/10.1021/jp311471f

[34] Sukhara A., Vereshchagin O., Yatsyshyn M.: Visnyk Lviv Univ. Ser. Chem., 2018, **59**, 414. https://doi.org/10.30970/vch.5902.414
[35] Carlin R.: Magnetochemistry. Springer 1986. https://doi.org/10.1007/978-3-642-70733-9
[36] Kulhánková L., Tokarský J., Peikertová P. *et al.*: J. Phys. Chem. Solids., 2012, **73**, 1530. https://doi.org/10.1016/j.jpcs.2011.11.043
[37] Sathiyanarayanan S., Azim S., Venkatachari G.: J. Appl. Polym. Sci., 2008, **107**, 2224. https://doi.org/10.1002/app.27254
[38] Shao L., Qiu J., Liu M. *et al.*: Synth. Met., 2010, **160**, 143. https://doi.org/10.1016/j.synthmet.2009.10.022
[39] Chae H., Zhang W., Piao S., Choi H.: Appl. Clay Sci., 2015, **107**, 165. https://doi.org/10.1016/j.clay.2015.01.018
[40] Buckley H., Bevan J., Brown K. *et al.*: Mineral. Mag., 1978, **42**, 373.
[41] Kazim S., Ahmad S., Pfleger J. *et al.*: J. Mater. Sci., 2012, **47**, 420. https://doi.org/10.1007/s10853-011-5815-y
[42] McRae S.: Earth-Sci. Rev., 1972, **8**, 397. https://doi.org/10.1016/0012-8252(72)90063-3
[43] Yatsyshyn M., Makogon V., Reshetnyak O., Błażejowski J.: Structure and Thermal Stability of Silica-Glauconite/Polyaniline Composite [in:] Reshetnyak O., Zaikov G. (Eds.), Computational and Experimental Analysis of Functional Materials. Apple Academic Press, CRC Press (Taylor & Francis Group), Toronto, New Jersey 2017, 497. https://doi.org/10.1201/9781315366357
[44] da Oliveira R., Bizeto M., Camilo F.: Carbohyd. Polym., 2018, **199**, 84. https://doi.org/10.1016/j.carbpol.2018.06.049
[45] Kolodii M., Vereshchagin O., Yatsyshyn M., Reshetnyak O.: Pratsi Naukovoho Tovarystva im. Shevchenka. Khimichni nauky, 2019, **56**, 92.
[46] Bhadra S., Singha N., Khastgir D.: Eur. Polym. J., 2008, **44**, 1763. https://doi.org/10.1016/j.eurpolymj.2008.03.010
[47] Doca N., Vlase G., Vlase T. *et al.*: J. Therm. Anal. Calorim., 2009, **97**, 479. https://doi.org/10.1007/s10973-009-0217-y
[48] Yatsyshyn M., Dozhdzhanyk V., Nesterivs'ka S. *et al.*: Pratsi Naukovoho Tovarystva im. Shevchenka. Khimichni nauky, 2019, **56**, 101.
[49] Vohra S., Kumar M., Mittal S., Singla M.: J. Mater. Sci: Mater. Electron., 2013, **24**,1354. https://doi.org/10.1007/s10854-012-0933-0
[50] Patil K., Zope P., Patil U. *et al.*: Bull. Mater. Sci., 2019, **42**, 24. https://doi.org/10.1007/s12034-018-1705-0
[51] Kulhánková L., Tokarský J., Matějka V. *et al.*: Thin Solid Films, 2014, **562**, 319. https://doi.org/10.1016/j.tsf.2014.05.006
[52] Saldan I., Stetsiv Y., Makogon V. *et al.*: Chem. Chem. Technol., 2019, **13**, 85. https://doi.org/10.23939/chcht13.01

ВЛАСТИВОСТІ КОМПОЗИТІВ ПРИГОТОВЛЕНИХ З ГЛАУКОНІТУ ТА ПОЛІАНІЛІНУ У ВОДНИХ РОЗЧИНАХ ФОСФАТНОЇ КИСЛОТИ

Анотація. *Окисненням аніліну з використанням амоній пероксидисульфату у водних розчинах фосфатної кислоти на поверхні порошкоподібного глауконіту приготовлені глауконіт-поліанілінові композити. За допомогою Х-променевої дифракції та ІЧ спектроскопії з перетворенням Фур'є підтверджено міжмолекулярну взаємодію між аморфними макромолекулами поліаніліну та міжфазне зв'язування поліаніліну до поверхні глауконіту. Встановлено, що збільшення концентрації фосфатної кислоти приводить до більш міцного міжмолекулярного та міжфазного контакту через водневий зв'язок, наслідком чого є вища електропровідність, але не має впливу на магнітну сприйнятливість композитів. З використанням термічного аналізу підтверджено міжфазну взаємодію між макромолекулами поліаніліну та поверхнею порошкоподібного глауконіту.*

Ключові слова: *композит глауконіт-поліанілін, структура, електрична провідність, магнітна сприйнятливість, термічна стабільність.*